Indoor Granular Presence Sensing and Control Messaging With an Ultrasonic Circular Array Sensor

Shahrzad Naghibzadeh, Ashish Pandharipande, *Senior Member, IEEE*, David Caicedo, and Geert Leus, *Fellow, IEEE*

***Abstract*— Providing automated granular control of lighting, along with user-driven control, results in an energy-efficient smart lighting system design while catering to personal occupant preferences. Two functional ingredients in such a system are: 1) sensing that provides granular information on occupant location and 2) a communication system to transmit control messages from a user. In this paper, we consider an ultrasonic circular array sensor that provides the dual functionality of granular occupant sensing and a communication receiver for user control transmissions. A ceiling-mounted sensor configuration with a colocated ultrasonic transmitter and array receiver is considered. To perform presence sensing, this transmitter sends periodic bursts of sinusoidal pulses that, upon reflection from the environment, are received at the array sensor. The echoes are processed to obtain estimates of range, azimuth, and elevation angles corresponding to possible occupant movements. A Kalman filter based on a near constant velocity model is used for target tracking. The resulting occupant location is used for energy-efficient lighting control. A user may in addition control lamps in its vicinity by sending messages at ultrasonic frequency, which are processed by the receiver array, and used to further adapt requested parameters of the lighting system. The proposed sensing and messaging solution is tested in an indoor office space with an eight-element receiver array sensor prototype.**

***Index Terms*— Ultrasonic circular array sensors, indoor granular presence sensing, Kalman tracking, ultrasonic communication, lighting control.**

I. Introduction

THE design of energy-efficient lighting systems is important, given that electric lighting is a major constituent of electricity consumption in office buildings [1]. An approach to saving energy is by providing illumination at a prescribed level only in occupied regions and providing lower illumination levels in unoccupied regions. Control schemes have been designed with these illumination objectives [2], [3]. A key ingredient in this approach is granular presence sensing, i.e. coarsely determining spatial occupancy in a given space. While energy efficiency is an important design consideration, catering to individual user illumination needs is equally important. Thus providing occupants with the ability to control lighting to meet individual needs is necessary. Control schemes may then take specific user inputs into consideration to enhance user satisfaction with the rendered illumination [4]–[6]. In this paper, we present an ultrasonic system to provide the functionalities of granular presence sensing and user communication in a smart lighting system.

Ultrasonic sensors are attractive for indoor presence detection since they can offer greater sensitivity over a larger detection region as compared to passive infrared sensors [7] at comparable costs. Traditional passive infrared sensors [7] only provide binary occupancy information and cannot localize users. An ultrasonic array sensor when operated in pulsed mode can provide range as well as angular information [8]–[10]. Ultrasonic linear array sensors were considered for localized presence sensing [8] in a wall-mounted configuration. Under a ceiling-mounted configuration, which is typical in indoor lighting control applications, these sensors were proposed for improved presence detection [9] and one-dimensional zoning [10]. With a linear array sensor in a ceiling-mounted configuration, it is only possible to obtain information on the half-plane elevation angle. A uniform circular array can, on the other hand, provide 360° azimuth angle as well as half-plane elevation angle information. Together with range, an occupant may thus be localized in a two-dimensional horizontal plane. Ultrasonic sensor systems in different system configurations have been used in [11] and [12] for indoor ranging and reference-free localization. In addition, ultrasonic sensors have been used for indoor communications [13]–[17]. A high rate ultrasonic communication system was designed to operate in frequencies in the order of hundreds of kHz [13], [14], while in [15] a bandwidth between 50-110 kHz was used for transmission. In [16] and [17], the feasibility of ultrasonic communications at frequencies in the order of tens of kHz was investigated.

The proposed ultrasonic system consists of an ultrasonic circular array sensor, situated at the ceiling, and a user device capable of ultrasonic transmissions at a frequency within the bandwidth of the array sensor. The ultrasonic circular array

Manuscript received January 16, 2015; accepted May 4, 2015. Date of publication May 8, 2015; date of current version July 13, 2015. The associate editor coordinating the review of this paper and approving it for publication was Dr. Thilo Sauter.

S. Naghibzadeh is with Philips Research, High Tech Campus, Eindhoven 5656AE, The Netherlands, and also with the Delft University of Technology, Delft 2628CD, The Netherlands (e-mail: s.naghibzadeh@tudelft.nl).

A. Pandharipande and D. Caicedo are with Philips Research, High Tech Campus, Eindhoven 5656AE, The Netherlands (e-mail: ashish.p@philips.com; david.caicedo@philips.com).

G. Leus is with the Delft University of Technology, Delft 2628CD, The Netherlands (e-mail: g.j.t.leus@tudelft.nl).

Color versions of one or more of the figures in this paper are available online at http://ieeexplore.ieee.org.

Digital Object Identifier 10.1109/JSEN.2015.2431373

sensor has a co-located single transmitter and a wideband circular array receiver. The transmitter sends pulsed sinusoids at a frequency that is within its bandwidth (for instance, commercial ultrasonic transmitters used in lighting control applications have a typical center frequency of 40 kHz). The circular array processes the received signal obtained after reflection from objects in the environment to obtain granular presence information, which is passed to the lighting controller, designed for providing pre-determined illumination levels in the occupied and unoccupied regions.

To obtain granular presence, the sampled raw received signal is first preprocessed through a moving target indicator (MTI) processor. In MTI processing, echoes received over two consecutive pulse intervals are subtracted in order to suppress static clutter. Afterwards, range information of potentially moving targets is extracted using a power detector applied to the downmixed MTI-processed difference signal. A conventional beamformer [18] is then applied to the data in ranges with detected movements to obtain azimuth and elevation angles with respect to the sensor. From the estimated range and angles of arrival, location estimates are obtained. These are converted to Cartesian coordinates, so that a linear tracker may be used, and supplied to the tracking algorithm. The algorithm first associates measurements in each scan with tentative tracks based on a coarse gate [19] and a proximity-based clustering algorithm. The tracks are then filtered through a Kalman filter based on a near constant velocity (NCV) motion model [20]. To each tentative track, a score is assigned that consists of a signal-related term, and a kinematic term. In order to confirm tentative tracks as true targets and delete tracks that have been lost for a number of scans, two corresponding thresholds are computed. Furthermore, for tracks in sufficiently close neighborhood, a track merger is applied that compares the state estimate of tracks and if for some number of scans the state estimates stay close, the redundant track is dropped. Initial results of granular presence sensing were presented in our earlier conference paper [21].

An occupant may change lighting system characteristics, such as illumination level or color level, by communicating with the ultrasonic array sensor. At the occupant side, there is a user device capable of producing ultrasonic transmissions. For instance, a commercial audio speaker of a laptop or smartphone may be used; most speakers may be used at ultrasonic frequencies in the range of 18-22 kHz [22], [23]. We use 5 bits to encode user requests (e.g. increase or decrease illumination level by a specific amount) using on-off keying (OOK). Line-of-sight is assumed during user signalling, as is common in remote control actions. At the circular array receiver, the communication signal is bandpassed. The signal is decoded and DoA is performed to determine the region from which the message was received. This information is then sent to the lighting controller where the requested user changes are executed.

We evaluate the performance of the proposed sensing and communication solution in an indoor office environment with an 8-element uniform circular array prototype and a laptop for signalling from the user.

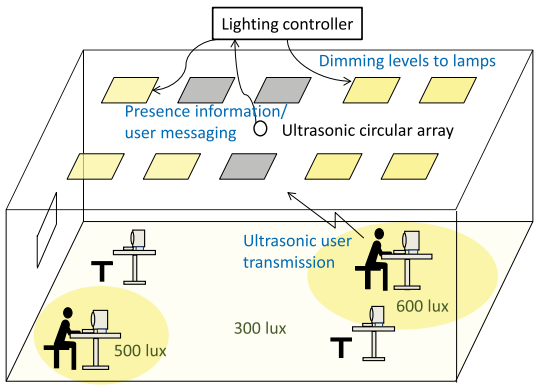

Fig. 1. Illustration of ultrasonic sensing/communication system for lighting controls.

II. System Description

The ultrasonic system for granular presence sensing and user messaging is shown in Fig. 1. The ultrasonic array sensor, consisting of a transmitter and co-located circular array, is situated at the ceiling of the room. It serves two functions: one, for granular presence sensing, and two, as an ultrasonic communication receiver. In the function of granular presence sensing, the sensor is used to determine where potential occupants are situated. This information is then provided to the lighting controller to achieve automatic localized illumination; a prescribed level of average illuminance (e.g. 500 lux) may be provided around the occupied region and a lower average illuminance level (e.g. 300 lux) may be provided in unoccupied regions. In the function of a communication receiver, the array sensor decodes the user message transmitted from a user-equipped device and also determines the region from where the message was transmitted. The user message information is then conveyed to the lighting controller to achieve user-controlled localized illumination, and adjust parameters of appropriate lamps in the lighting system (for e.g. dimming up so that a higher average illuminance level of 600 lux may be provided to this user). Control algorithms to adapt dimming of lamps to meet illuminance constraints have been investigated in [2] and [4]–[6] under different system settings. The user-equipped mobile device that acts as an ultrasonic transmitter may be a commercial speaker of a smartphone or laptop.

The ultrasonic transmitter used for presence sensing has a broadbeam pattern and a narrow bandwidth with center frequency $f_{c,1}$. The speaker of each user-equipped mobile device is set to operate at the near-ultrasonic central frequency of $f_{c,2}$, where frequencies $f_{c,1}$ and $f_{c,2}$ are sufficiently apart to avoid any interference. The receiver array is made of M individual MEMS components that are sensitive to ultrasonic frequencies. Their compact size permits construction of a uniform circular array with limited spatial aliasing (the inter-element separation is close to half-wavelength, albeit higher). The array sensor is located at the ceiling, a configuration that is common in indoor lighting control applications [2], [10]. We assume without loss of generality that the origin of the coordinate system is at the sensor.

A. Circular Array Sensor

The receiver is a circular array with M elements uniformly distributed on a circle with radius r. For presence sensing purposes, the receiver processes signals at the central frequency, $f_{c,1}$, of the co-located ultrasonic transmitter. For receiving user control messages, the receiver processes signals around the central frequency, $f_{c,2}$, of the mobile devices. A spherical coordinate system with origin at the center of the receiver is considered for direction of arrival (DoA) estimation of the backscattered plane waves. Elevation angles in the range $\theta \in [0, \pi/2]$ are measured with respect to the positive direction of the z-axis, which in our case is directed from the ceiling towards the floor. Azimuth angles of the impinging plane waves are in the range of $\phi \in [0, 2\pi)$ and are measured counterclockwise from the x-axis in the $x-y$ plane of the ceiling. The reader is referred to [24] (Fig. 4 therein) for a depiction of the elevation and azimuth angles.

Assuming the alignment of the first array element with the positive direction of the x-axis, the angular position of the array elements and the relative delay in the reception of the wavefront with respect to the origin of the array are respectively given by [20], [24]

$$\phi_m = 2\pi\left(\frac{m-1}{M}\right), \quad m = 1, 2, \ldots, M,$$
$$\tau_m = -\frac{r}{v_s}\sin(\theta)\cos(\phi - \phi_m), \quad m = 1, 2, \ldots, M. \tag{1}$$

Therefore, the element-space circular array response is given by the steering vector:

$$\boldsymbol{a}(\theta, \phi) = \begin{pmatrix} \exp[\mathbb{j}\frac{2\pi}{\lambda} r \sin\theta \cos(\phi - \phi_1)] \\ \exp[\mathbb{j}\frac{2\pi}{\lambda} r \sin\theta \cos(\phi - \phi_2)] \\ \vdots \\ \exp[\mathbb{j}\frac{2\pi}{\lambda} r \sin\theta \cos(\phi - \phi_M)] \end{pmatrix}, \tag{2}$$

where $\lambda = v_s/f_{c,1}$ is the wavelength, exp represents the exponential function, and $\mathbb{j} = \sqrt{-1}$.

III. Granular Presence Sensing

A. Transmitted Waveform

The transmitter sends out periodic pulsed sinusoids [8], [9], with an active transmission duration of T_s and pulse repetition interval being T_p. The transmitted signal can be written as a real-valued bandpass signal with center frequency $f_{c,1}$ as

$$s(t) = Re\{u(t)\exp[\mathbb{j}2\pi f_{c,1} t]\}, \tag{3}$$

where $Re\{.\}$ represents the real part, and

$$u(t) = \begin{cases} 1 & 0 < t - \lfloor \frac{t}{T_p} \rfloor T_p \leq T_s \\ 0 & T_s < t - \lfloor \frac{t}{T_p} \rfloor T_p \leq T_p \end{cases}. \tag{4}$$

Two pulse repetition intervals constitute a scan. In (3), T_p is an integer multiple of $1/f_{c,1}$.

This section describes the signal processing applied to the raw received signal to estimate the occupant location and form the measurements to supply to the tracker. First, the received signal is demodulated and converted to baseband. Then, MTI processing is applied to suppress the effect of static clutter. Subsequently, range values corresponding to possible occupant movements are estimated by applying a power detector on the clutter-suppressed difference signal. In the next step, data from the tentative target range is provided to a beamformer to extract azimuth and elevation angles of arrival. Thereafter, the measured locations in spherical coordinates are converted to Cartesian coordinates and used as input to the tracker. The various receiver processing steps are illustrated in Fig. 2.

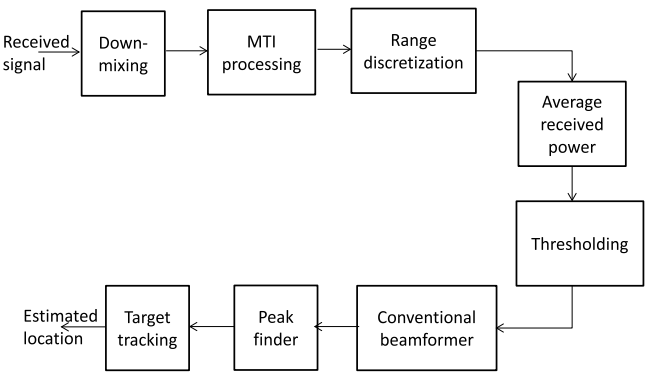

Fig. 2. Block diagram of receiver sensor processing.

B. Practical Design Considerations

The target detection area that the sensor should achieve is 40-50 m^2, at a mounting height of 2.5-3 m, considering typical topologies of cellular offices and zones in open offices. For the office space considered in our experiments, the maximum range to be covered by the sensor is approximately 6 m. Considering the speed of sound in air to be $v_s = 343$ ms^{-1} and given the center frequency of the transmitted narrowband waveform is $f_{c,1} = 40$ kHz, the wavelength $\lambda \approx 8.6$ mm.

We considered an 8-element uniform circular array so as to have a reasonable spatial granularity while keeping the sensor complexity low. Due to the size of available commercial components used to construct the receiver array, the inter-element spacing is 4.6 mm. Since this value is slightly higher than the half-wavelength, we expect to have some spatial aliasing in the form of spatial sidelobes in the beam pattern. This needs to be alleviated in the receiver processing so as to avoid falsely detecting non-existent occupants.

In order to treat spherical wavefronts as plane waves, a user is required to be in the far field of the array sensor [25]. Given that the circular array has a radius $r \approx 6$ mm, and with a mounting height of 3 m, the far field conditions are satisfied.

The duration of the pulsed sinusoid is chosen as $T_s = 4$ ms, so as to provide a reasonable range resolution of 0.68 m [8]. In order to guarantee unambiguous range measurements, a quiet period has to be scheduled so that echoes from the environment die before the transmission of the next pulsed sinusoid and sufficiently large to sense over the required range. Thus, a pulse repetition interval of $T_p = 60$ ms was chosen in order to cover the maximum range and allow for the reception of all possible echoes.

C. Conversion to Baseband

The received signal at the receiver elements is a real-valued bandpass signal represented as

$$w_m(t) = Re\{g_m(t)\exp[\jmath 2\pi f_{c,1} t]\}$$

where $w_m(t)$ is the received signal at the mth element and $g_m(t)$ is the baseband received signal. Due to multipath caused by static and moving clutter in the indoor environment, the sinusoidal pulse is received from multiple paths with different attenuation, delay and Doppler shift and it is the sum of multiple such echoes. In order to down-convert the received signal to baseband, the received signal is multiplied with the complex exponential $\exp[-\jmath 2\pi f_{c,1} t]$ [26] and a lowpass filter is applied with cut-off frequency $f_{D,max}$ to allow for Doppler shifts.

D. Moving Target Indicator Processing

The baseband received signal at the mth element at time instant t (where $0 \leqslant t < T_p$) is composed of $N(t)$ components and can be expressed as

$$g_m(t) = \sum_{n=1}^{N(t)} \beta_{m,n}(t) u(t - T_{m,n}(t)) \exp[-\jmath 2\pi f_{c,1} T_{m,n}(t)] \times \exp[\jmath 2\pi f_{D_{m,n}}(t)] + \zeta_m(t), \quad (5)$$

where $N(t) = N_1(t) + N_2$ is composed of $N_1(t)$ components due to moving clutter and N_2 components due to static clutter, $\beta_{m,n}(t)$ denotes the attenuation factor of the nth path with respect to the mth array element, and $\zeta_m(t)$ is the additive white Gaussian noise at the mth element. The terms $T_{m,n}(t)$ and $f_{D_{m,n}}(t)$ are respectively the time delay and Doppler shift of the nth path at time t and are given by

$$T_{m,n}(t) = \frac{2d_{m,n}(t)}{v_s}, \quad f_{D_{m,n}}(t) \approx \frac{2v_{m,n}(t)}{\lambda},$$

where $d_{m,n}(t)$ is the nth path length and $v_{m,n}(t)$ is the radial speed of the object that has caused the echoes with respect to the mth array element.

We apply single canceller MTI processing [26], based on the subtraction of echoes received over two consecutive pulse intervals (called a scan), to suppress the effect of static clutter. The MTI processor subtracts the echo received at a time instant t from the corresponding echo received at the next pulse repetition interval. That is, for the mth element,

$$\Delta g_m(t) = g_m(t + T_p) - g_m(t).$$

For echoes caused by static objects, the Doppler frequency is zero, and since path delay does not change over time, the difference signal after MTI processing due to received signals from static objects is zero. Therefore, the difference signal only contains $N_1(t)$ components. Assuming that the environment characteristics and the speed of the objects caused by each component are constant over a scan, the gain difference of the nth echo component, $\beta_{m,n}(t+T_p) - \beta_{m,n}(t)$, can be zero for certain blind speeds [8], underlying the need for tracking so as not to lose track of occupant movements.

E. Range Processing

To detect the location of the occupants in the office room, we first extract range information from the received echo. For the purpose of practical implementation, we discretize the range covered over a scan duration into a number of range bins. The size of the range bins will determine the range measurement granularity of our system. We choose the size of each range bin to be $\Delta d = 0.343$ m. Since the signal is digitized at the receiver with sampling frequency $f_{s,1}$, the ϱth range bin contains $\nu = \lfloor \frac{2\Delta d f_{s,1}}{v_s} \rfloor$ samples.

Let the downmixed and MTI-processed portion of the received signal at the mth array element for sample ς at the ϱth range bin be denoted as $\overline{\Delta g}_m(\varrho, \varsigma)$, $\varsigma = 1, 2, \ldots, \nu$. The preprocessed signal at the ϱth range bin for ςth sample received by M elements is then given by

$$\overline{\boldsymbol{\Delta g}}(\varrho, \varsigma) = \left[\overline{\Delta g}_1(\varrho, \varsigma), \overline{\Delta g}_2(\varrho, \varsigma), \ldots, \overline{\Delta g}_M(\varrho, \varsigma)\right]^T.$$

To detect movement, the average received power per range bin received over all the elements is computed as

$$\Gamma(\varrho) = \frac{1}{M\nu} \sum_{m=1}^{M} \sum_{\varsigma=1}^{\nu} |\overline{\Delta g}_m(\varrho, \varsigma)|^2. \quad (6)$$

The amount of received power would depend on the size of user movement, but also on aspects like human body orientation and the type of clothing. The power per range bin is then compared against a threshold. The detection threshold $\delta(\varrho)$ per range bin ϱ is set using the noise power, $\epsilon(\varrho)$, measured when the environment is unoccupied, so as to achieve a desired probability of false alarm (we choose a value of 10^{-3}).

Due to multipath propagation in the indoor environment, echoes from the same moving occupant reach the receiver with different delays in multiple range bins after power detection. We consider that the strongest echo is due to the line-of-sight component between the closest occupant and the sensor. In order to deal with the effect of multipath and since the number of occupants is not known a priori, we consider the following processing steps. First, the range bin with the maximum received power is chosen and compared against the corresponding detection threshold. Let ϱ_{max} denote the range bin with the maximum received power. If the following condition holds,

$$\Gamma(\varrho_{max}) > \delta(\varrho_{max}),$$

we conclude that the room is occupied. Thereafter, all other range bins with received power higher than or equal to $\frac{\Gamma(\varrho_{max})}{4}$ are compared against their corresponding detection threshold. More specifically, if for the ϱth range bin the following condition holds,

$$\Gamma(\varrho) \geq \max\{\delta(\varrho), \frac{\Gamma(\varrho_{max})}{4}\}, \quad (7)$$

then that range bin is declared as a possible range bin where an occupant is located and considered for further processing. This procedure may still allow multipath echoes to be declared as active range bins. The tracking algorithm is designed to correct some of these false detections. Also note from (7) that in order

to limit the amount of ranges that need to be further processed, we limit our attention to those echoes that are within a threshold of 6 dB (corresponding to a factor of 4 in (7)) with respect to the strongest signal power. This mechanism may reject true targets that are in further regions but that would be fixed in successive scans due to the movement of the occupants and with the help of the tracking mechanism that takes into account the temporal correlation of the detections relating to true targets.

F. DoA Processing

After range detection, a number of range bins are declared to contain occupants either due to the presence of a true target or due to multipath. The data from these range bins is then processed to find the angle of arrival of the source contained. A two-dimensional conventional beamformer is then applied on the preprocessed data corresponding to each of the active range bins. For the preprocessed data, $\overline{\boldsymbol{\Delta g}}(\varrho, \varsigma)$, at the ϱth active range bin for ςth sample, the two-dimensional angular spectrum is written as

$$\Lambda(\theta, \phi, \varrho) = \frac{1}{M\nu} \sum_{\varsigma=1}^{\nu} |\boldsymbol{a}^H(\theta, \phi)\overline{\boldsymbol{\Delta g}}(\varrho, \varsigma)|^2, \tag{8}$$

where Λ indicates the angular response and θ and ϕ take values from the discrete sets Θ and Φ respectively.

Taking into account that in each range bin at most one occupant movement is of interest, the maximum of the angular spectrum (which corresponds to the angular location where the maximum power is received) is found. Furthermore, the signal-to-noise ratio (SNR) at the detected location is computed as

$$\bar{\eta} = \eta(\theta_{max}, \phi_{max}, \varrho) = \frac{\max_{\theta\in\Theta, \phi\in\Phi} \Lambda(\theta, \phi, \varrho)}{\epsilon(\varrho)}, \tag{9}$$

where θ_{max} and ϕ_{max} are the angles with maximum received power. After DoA processing, the elevation angle, azimuth angle, measured SNR at the location and the corresponding range bin which are denoted respectively as

$$\{\theta_{max}, \phi_{max}, \varrho, \bar{\eta}\}$$

are stored to be supplied to the tracker for refining the location estimates by considering the temporal correlation of detections corresponding to the target.

G. Target Tracking

After range and DoA processing, the observation points collected in one scan are then transformed to Cartesian coordinates. Before being supplied to the tracking algorithm, data is filtered to disregard infeasible location estimates that lie beyond the physical boundaries of the environment. The tracking is performed in two dimensions (x, y). A true moving target is persistent in the tracking region for several scans [27]. As a result, persistent clutter and observations formed due to sidelobes of the circular array also are classified as being a tentative target, whereas false detections caused by random noise or clutter are not correlated in time. In order to minimize misclassification between persistent false targets and the true ones, tracking and a mechanism for scoring the different tracks is implemented [20]. Tracking is also useful in addressing the problem of intermittent detections due to the MTI-processor suppressing target echoes at certain speeds [8].

For the data association and tracking algorithm described in the rest of the section, *a priori* knowledge of the existence of multiple targets (whether true targets or caused by clutter or sidelobes) is assumed. The tracking algorithm is composed of four main parts; (a) observation-to-track association, (b) NCV Kalman filter-based track prediction, (c) track scoring and (d) maintenance of a list of tentative targets with their current state and tracking score.

1) Observation-to-Track Data Association: Observations formed in one scan are first clustered to initiate multiple tentative targets based on the proximity of the measurements. A coarse gate with size roughly equal to the area a human occupies in $x - y$ plane is used to ensure that detections due to different parts of the human target body are combined. A circular gate with radius $\sqrt{2}$ m is chosen. Measurements falling into the same proximity of one gate are clustered as one tentative target and their location is fused to produce one measured location for the corresponding target. The fusion rule for the measurements inside the same cluster at the kth scan for q_1 measurements falling in the same gate l is as follows

$$\hat{x}_l^{(k)} = \frac{\sum_{i=1}^{q_1} x_{i,l}^{(k)}\ \bar{\eta}_{i,l}^{(k)}}{\sum_{i=1}^{q_1} \bar{\eta}_{i,l}^{(k)}}, \quad \hat{y}_l^{(k)} = \frac{\sum_{i=1}^{q_1} y_{i,l}^{(k)}\ \bar{\eta}_{i,l}^{(k)}}{\sum_{i=1}^{q_1} \bar{\eta}_{i,l}^{(k)}}, \tag{10}$$

where $\bar{\eta}_{i,l}^{(k)}$ is the SNR per observation point i in the lth target gate and $(\hat{x}_l^{(k)}, \hat{y}_l^{(k)})$ is the initial estimated tentative target location at the kth scan. Coordinates of the tentative targets are stored and sent to the Kalman filter to be propagated to the next scan.

2) Filtering and Prediction: For track filtering, a NCV motion model [28] is used to model target movement dynamics together with a two-dimensional Kalman filter. The state of the lth tentative target at scan k is presented as

$$\boldsymbol{s}_l^{(k)} = \left[x_l^{(k)}, y_l^{(k)}, \dot{x}_l^{(k)}, \dot{y}_l^{(k)}\right]^T,$$

where $x_l^{(k)}$ and $y_l^{(k)}$ represent the occupant location and $\dot{x}_l^{(k)}$ and $\dot{y}_l^{(k)}$ represent its speed. Occupant movement must satisfy the kinematic motion equation [29]

$$\boldsymbol{p}_l^{(k)} = \frac{1}{2}\ddot{\boldsymbol{p}}_l^{(k-1)}(\Delta t)^2 + \dot{\boldsymbol{p}}_l^{(k-1)}(\Delta t) + \boldsymbol{p}_l^{(k-1)} \tag{11}$$

where $\dot{\boldsymbol{p}}_l^{(k-1)}$ and $\ddot{\boldsymbol{p}}_l^{(k-1)}$ respectively denote the initial speed and initial acceleration of the lth target at scan k, $\boldsymbol{p}_l^{(k)} = [x_l^{(k)}, y_l^{(k)}]^T$ denotes the position vector and $\Delta t = 2T_p$ denotes the time between scans. Therefore, the occupant state transition at scan k is written as

$$\boldsymbol{s}_l^{(k+1)} = \boldsymbol{A}\overline{\boldsymbol{s}}_l^{(k)} + \overline{\boldsymbol{w}}^{(k)} \tag{12}$$

where $\boldsymbol{A}$ is the state transition matrix expressed as

$$\boldsymbol{A} = \begin{bmatrix} 1 & 0 & \Delta t & 0 \\ 0 & 1 & 0 & \Delta t \\ 0 & 0 & 1 & 0 \\ 0 & 0 & 0 & 1 \end{bmatrix},$$

$\boldsymbol{s}_l^{(k+1)}$ is the state of the occupant at the following scan and $\overline{\boldsymbol{w}}^{(k)}$ denotes the process noise which is the uncontrollable input (occupant acceleration) to the modeled system. The NCV model gives the expression for the state error covariance matrix as [28]

$$\boldsymbol{Q}_s = \sigma_s^2 \begin{bmatrix} \Delta t^4/4 & 0 & \Delta t^3/2 & 0 \\ 0 & \Delta t^4/4 & 0 & \Delta t^3/2 \\ \Delta t^3/2 & 0 & \Delta t^2 & 0 \\ 0 & \Delta t^3/2 & 0 & \Delta t^2 \end{bmatrix},$$

with $\sigma_s = 1\ \text{ms}^{-2}$ is a chosen design value.

Let $\boldsymbol{z}_l^{(k)} = (\hat{x}_l^{(k)}, \hat{y}_l^{(k)})^T$ denote the combined measurement at scan k for the lth tentative target, since our system only measure target position and do not have information about its speed; the measurement and the state of the occupant are related as

$$\boldsymbol{z}_l^{(k)} = \boldsymbol{C}\boldsymbol{s}_l^{(k)} + \boldsymbol{e}^{(k)}, \tag{13}$$

where $\boldsymbol{C}$ is

$$\boldsymbol{C} = \begin{bmatrix} 1 & 0 & 0 & 0 \\ 0 & 1 & 0 & 0 \end{bmatrix}$$

and $\boldsymbol{e}^{(k)}$ is the measurement noise which is assumed to be white Gaussian with covariance matrix $\boldsymbol{Q}_e = \sigma_e^2 \boldsymbol{I}$, where $\boldsymbol{I}$ is a 2×2 identity matrix and variance $\sigma_e = 1$ m is chosen. Matrices $\boldsymbol{Q}_s$ and $\boldsymbol{Q}_e$ are parameters in the prediction steps of a Kalman filter [30].

Upon receipt of data in a scan, the data within each (tentative) target gate is specified and the state of the target is updated using the received data within its gate and propagated ahead using the Kalman filter [30] to predict the occupant state at the following scan. The predicted location at the following scan forms the center of the corresponding target gate. In order to update the state of a (tentative) target and avoid merging of two crossing targets, the observation which is closest in distance to the predicted position of a target is chosen. Let $\boldsymbol{z}_{i,l}^{(k)} = [\hat{x}_{i,l}^{(k)}, \hat{y}_{i,l}^{(k)}]^T$ denote the ith observation at the lth target gate at scan k and $\hat{\boldsymbol{p}}_l^{(k|k-1)} = [\hat{x}_l^{(k|k-1)}, \hat{y}_l^{(k|k-1)}]^T$ denotes the predicted target location from the previous scan, the chosen measurement to update the target state is

$$\boldsymbol{z}_l^{(k)} = \min_i \|\hat{\boldsymbol{p}}_l^{(k|k-1)} - \boldsymbol{z}_{i,l}^{(k)}\|. \tag{14}$$

If there are measurements remaining which do not belong to any existing target gate, new tentative targets are formed by combining the measurements based on weighted average of the measurements inside the new gate in the same manner as discussed in Section III-G1.

Each of the observations at the current scan are assumed to have a normal distribution, $\mathcal{N}(\hat{\boldsymbol{p}}_l^{(k|k-1)}, \bar{\boldsymbol{Q}}_l^{(k|k-1)})$, around the predicted position, where $\bar{\boldsymbol{Q}}_l^{(k|k-1)}$ denotes the related noise covariance matrix. In order to represent (a) the confidence in a tentative track as being a true target, (b) evaluate observation-to-track updates and (c) have a mechanism to initiate true tracks and delete false tracks or targets that have disappeared, a tracking score is used. The tracking score consists of a kinematic term and a signal-related term. The kinematic term is related to the distance of the detection from the center of the corresponding gate and the signal-related term is the SNR at the location where the detection was formed.

Let $d_{i,l}^{(k)}$ denote the distance of the ith measured location at scan k corresponding to the lth target from the predicted position $\hat{\boldsymbol{p}}^{(k|k-1)}$ and $\bar{\eta}_{i,l}^{(k)}$ denote the SNR measured at that location. A score is assigned to each of the measurements within the lth target gate as

$$\Omega_{i,l}^{(k)} = \varrho_{i,l}^2 \bar{\eta}_{i,l}^{(k)} e^{-d_{i,l}^{(k)}}, \tag{15}$$

where $\varrho_{i,l}$ is the range bin corresponding to the lth target. Since signal power drops with the square of distance to the transmitter due to path loss, we include the factor $\varrho_{i,l}^2$ in the score in (15) in order to compensate for the power drop make it independent of range.

Thereby, the tracking score for the lth target at scan k is computed as

$$\hat{\Omega}_l^{(k)} = \min\{1, \hat{\Omega}_l^{(k-1)} + \max_i\{\Omega_{i,l}^{(k)}\}\}, \tag{16}$$

where $\hat{\Omega}_l^{(k-1)}$ denotes the tracking score at the previous scan. If in a cycle there remain unassociated measurements, they are supplied to the clustering algorithm to define new tentative targets. For the newly formed target clusters, $\hat{\Omega}_l^{(k-1)}$ is zero.

The data at scan k for each (tentative) target corresponding to the predicted state, error covariance matrix, previous locations of the target and tracking score are stored for use in the following scan.

3) Track Maintenance (Initiation, Deletion, Merging): By using the track score for (tentative) targets that includes a contribution from the SNR, the detection threshold can be set lower to allow for more detections, whether false or true [20]. The SNR-related term in the tracking score will ensure false track mitigation in the track confirmation step of the algorithm. Therefore, based on the tracking score of the targets, two thresholds are set to classify targets as tentative, confirmed or deleted. In the track maintenance process there are two main hypotheses [20]:

$$\mathcal{H}_0 : \text{Track is false}; \quad \mathcal{H}_1 : \text{Track is true}.$$

Based on these hypotheses, two thresholds are set for confirmation or deletion of tracks. Knowing that detections from a true target must be persistent over time, a timing constraint is also introduced to lower the probability of false target acceptance.

Note that due to the MTI processing, a small value of signal power, in (6), may be due to an occupant who is not moving or the absence of an occupant. We need to distinguish between these two situations while limiting rejection of true target rejections. In order to reduce true target rejection, we introduce a procedure before deciding that an occupant has left the sensing region. If in one scan no measurement is received for a target, the score of the corresponding target is decreased by a factor α, with $0 \leqslant \alpha \leqslant 1$, i.e. $\hat{\Omega}_l^{(k)} = \alpha \hat{\Omega}_l^{(k-1)}$ and is compared to the deletion threshold δ_1 for a pre-specified number of scans κ_1 before being disregarded. First, let us consider a scenario where an occupant has left the sensing region and the last detection associated to the target has a tracking score

of 1 (maximum tracking score). Because there is no occupant present, no signal associated with the target will be observed and the tracking score will not be increased. In order to ensure that the target is eventually dropped, we decrease the tracking score at each scan by the factor α. When the tracking score is smaller than the threshold δ_1 over at least κ_1 scans we decide to drop the target. Second, let us consider a scenario where an occupant has stopped moving and the last detection associated to the target has a tracking score of 1. Similar to the first scenario, no signal associated with the target will be observed and the tracking score will not be increased. If we use the same procedure, then a true target is rejected if the occupant does not move for long enough such that the associated tracking score goes below threshold δ_1 for at least κ_1 scans. Under this scenario, the required number of scans is given by

$$\tilde{\kappa} = \lceil \frac{\log \delta_1}{\log \alpha} \rceil + \kappa_1,$$

where $\lceil \frac{\log \delta_1}{\log \alpha} \rceil$ is the number of scans required for a tracking score of 1 to go below threshold δ_1 using a forgetting factor α. If we assume that the probability that an occupant does not move at each scan is independent of other scans and is equal to p, the probability of true target rejection is reduced to $p^{\tilde{\kappa}}$. Therefore, the described procedure ensures a low probability of true target rejection. A large α reduces the probability of true target rejection but also increases the time before deciding that a target has left the sensing region.

The track maintenance logic is as follows:

$\hat{\Omega}_l \leqslant \delta_1$ for κ_1 scans: Accept $\mathcal{H}_0$ (delete track l)

$\hat{\Omega}_l \geqslant \delta_2$ for κ_2 scans: Accept $\mathcal{H}_1$ (confirm track l)

$\delta_1 < \hat{\Omega}_l < \delta_2$: continue test (tentative target)

Here δ_1 and δ_2 are respectively track deletion and track confirmation thresholds, and κ_1 and κ_2 are the number of test scans for deletion and confirmation of the track respectively. The parameters δ_1, δ_2, κ_1 and κ_2 are chosen based on requirements of the system, e.g. latency and false alarm rate. δ_1 is set above δ_2 so that tracks caused by clutter and side lobes that are persistent in time but have a smaller tracking score than true targets would be tracked, but not initiated as true targets, at this step of the algorithm.

Furthermore, a track merging logic is applied for the situations when two closely-spaced tracks are formed due to initiation of tracks from different parts of the same human target body. In order to assure that the merger does not merge crossing targets, a logic based on the closeness of state vector of different (tentative) targets is used as follows

$$\|\overline{\boldsymbol{s}}_j - \overline{\boldsymbol{s}}_i\| < C_{th} \text{ for } \kappa_3 \text{ scans} \Rightarrow \text{drop the redundant track}$$

where $\overline{\boldsymbol{s}}_j$ and $\overline{\boldsymbol{s}}_i$ are the state estimates of the jth and ith track respectively and the redundant track refers to the track that has existed for a shorter time.

IV. Combined Control Messaging and Positioning

A. Transmitter

The transmitter chain is illustrated in Fig 3. A lighting control command is first translated into a binary sequence $\{b_k\}$

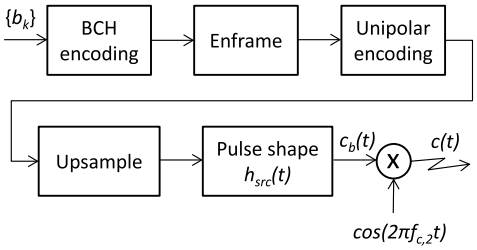

Fig. 3. Transmitter block diagram.

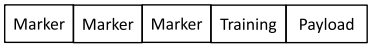

Fig. 4. Data frame structure.

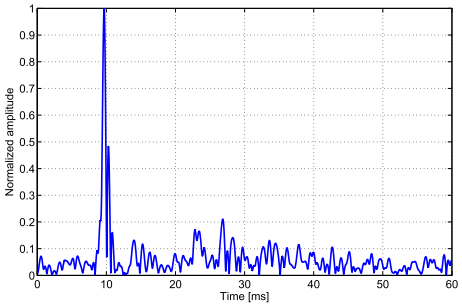

Fig. 5. Typical LOS channel in the test room.

of length L_1. After encoding the sequence with BCH error correcting code, the resulting encoded sequence of length L_2 is en-framed. The data frame consists of a preamble part (markers and training) and the payload part, as shown in Fig 4. The framed data is then transformed into unipolar voltage level and up-sampled to the speaker sampling frequency of $f_{s,2}$. Thereafter, the square-root raised cosine function $h_{src}(t)$ is assigned to the unipolar base-band data signal, multiplied with the carrier frequency at $f_{c,2}$ and transmitted through the mobile device speaker. The transmitted OOK signal is represented by [31]

$$c(t) = A_c c_b(t) cos(2\pi f_{c,2} t), \tag{17}$$

where $c(t)$ is the transmitted signal, $c_b(t)$ is the baseband transmitted pulse and A_c indicates the amplitude of the signal.

B. Indoor Ultrasound Channel

We assume that the orientation of the mobile device is such that a clear line-of-sight (LOS) path exists between the transmitter and the array receiver. A typical LOS channel response in the test office is shown in Fig. 5. It can be seen that the signal from the LOS path is received with significantly higher amplitude than other multipath components.

C. Receiver

1) Signal Detection: In order to detect the presence of a signal at the operating frequency $f_{c,2}$, the receiver uses power detection. It performs bandpass filtering on a time window of received samples, integrates the received power over that

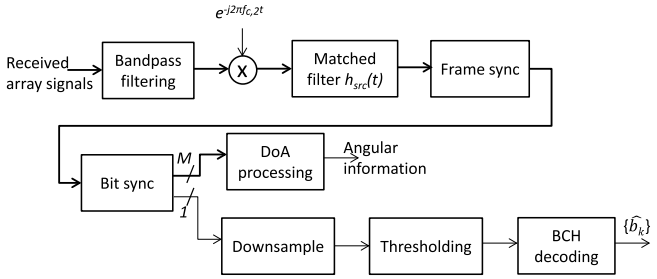

Fig. 6. Receiver block diagram.

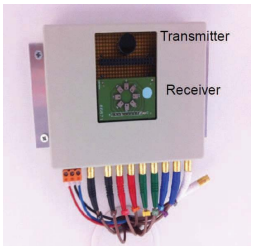

Fig. 7. Sensor prototype at ceiling.

time window and compares it with the detection threshold that is set above the bandpass noise power. Upon detection of the signal, a portion of the buffered and upcoming samples, which roughly correspond to the size of a data packet, are chosen for further processing.

2) Decoding and DoA Processing: The receiver implements a non-coherent detection followed by DoA processing and decoding, as illustrated in Fig 6. The received data block through the M receiver channels, sampled at the receiver sampling frequency $f_{s,2}$, is first complex conjugate demodulated with the zero-phase reference signal $\exp[-\jmath 2\pi f_{c,2}t]$ and passed through the matched filter that is matched to the square-root raised cosine $h_{src}(t)$ pulse shape of the transmitted baseband pulse. After conversion to baseband, it is determined whether the data block actually contains a data frame, and if so, frame and bit synchronization is performed. For this, the preamble structure is used. The preamble consists of three identical high-auto-correlation sequences (denoted as marker) and a training sequence as shown in Fig 4. First, a cross-correlation of the bandpass received data samples with the known marker sequence upsampled to the receiver sampling frequency is carried out. Three consecutive correlation peaks are found and compared against a threshold to maintain coarse timing synchronization [32]. The cross-correlation synchronization finds the coarse bit time of the first bit in the training sequence. Since the training sequence is known, a search for the peak of the bit time is performed to maintain fine timing synchronization. After maintaining the bit time, a short block of the following samples of the data block are supplied to the DoA estimation algorithm explained in Section III to determine the angles from which the control command is received. Furthermore, the data block is downsampled to bit rate. To set an adaptive threshold for making the decision on the received downsampled voltage level corresponding to '0' or '1' bit, the average voltage level of the '0' bits as well as '1' bits in the training sequence are computed and the threshold is set in the middle of the two levels to ensure minimum bit error probability and equal bit error probability for '0' and '1'. Thereafter, BCH decoding is performed on the resulting binary sequence to reduce the random bit errors.

D. Practical Design Considerations

1) Modulation: Standard laptop and smart-phone speakers sample the audio streams at the sample rate of $f_{s,2} = 44.1$ kHz. In theory, according to the Nyquist sampling criterion, these speakers are capable of producing tones with frequencies as high as 22 kHz. However, laptop and mobile phone hardware are optimized for working at audible frequencies (well below 20 kHz) but are capable of producing inaudible frequencies up to 22 kHz [22], [23]. In [33], a device-centric indoor positioning system was described based on ultrasonic beaconing of Kasami codes and reception in the 18-22 kHz using a built-in iOS microphone at a user device. For the design of the communication system, the available frequency band was assumed to be 18-22 kHz. The carrier frequency was chosen in the center of the available frequency interval $f_{c,2} = 20$ kHz. The uniform circular array receiver has a wide-band sensitivity pattern that covers the aforementioned frequency range. In order to choose the baseband pulse duration, taking into account the available bandwidth, real-time implementation requirements and assuming an LOS channel, a bit rate of $r_b = 2$ kbps which corresponds to the bit duration of $T_b = 500$ μs was chosen. We use a square-root raised cosine pulse shape with roll-off factor 0.3 and span of 10 pulses. We assume that the user-driven command (for the control of lighting or other building room control) is translated into a binary sequence of length $L_1 = 5$ bits. The binary command is then encoded to a sequence of length $L_2 = 15$ bits using a BCH code of (5, 15, 7) that can correct up to 3 errors. Due to the complexity advantage of non-coherent receivers and difficulty of estimating the carrier phase without a physical link between the transmitter and the receiver array, non-coherent detection was chosen. A common modulation technique used for non-coherent detection is OOK [31]. At the receiver side, the bandpass signal is centered around the carrier frequency with a bandwidth large enough to take into account Doppler effects. For the marker sequence in the transmitted data frame, a Gold code of length L_2 is used. Moreover, the chosen training sequence has approximately the same number of zeros and ones.

V. Performance Evaluation

An 8-element uniform circular array prototype, as depicted in Fig. 7, was installed in a ceiling-mounted configuration in an office room. The dimensions of the room were: length of 7.6 m, width of 6 m and height 3 m. The origin was at the sensor at roughly the center of the ceiling (see Fig. 8 for location), i.e. $x = 0; y = 0; z = 0$. The transmitter was of model 400EP14D [34] at center frequency $f_{c,1} = 40$ kHz, bandwidth 2 kHz and with a broad-beam profile.

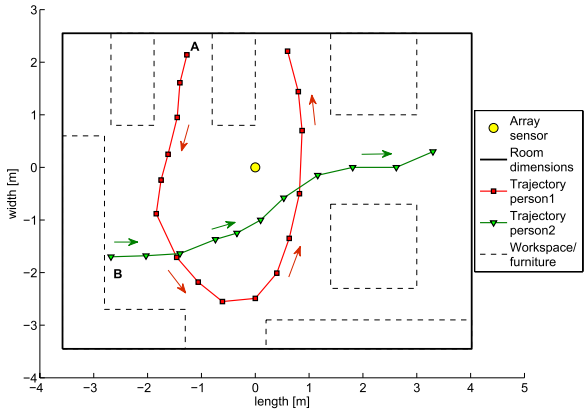

Fig. 8. Office room outline and trajectories of two occupants.

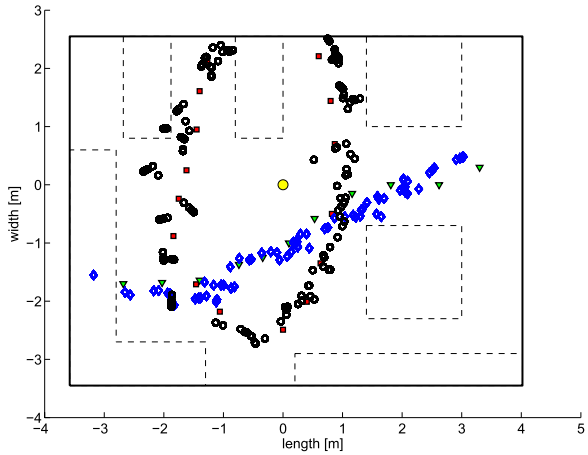

Fig. 9. Detection and tracking results in two occupants scenario.

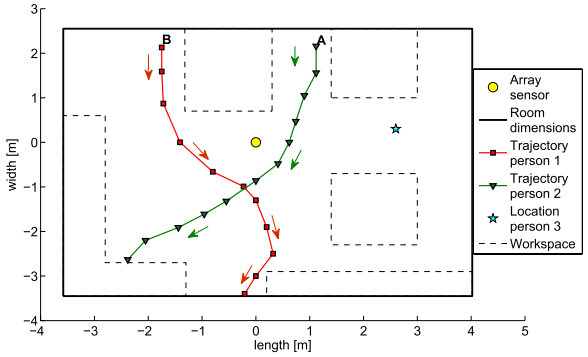

Fig. 10. Office room outline and trajectories of three occupants.

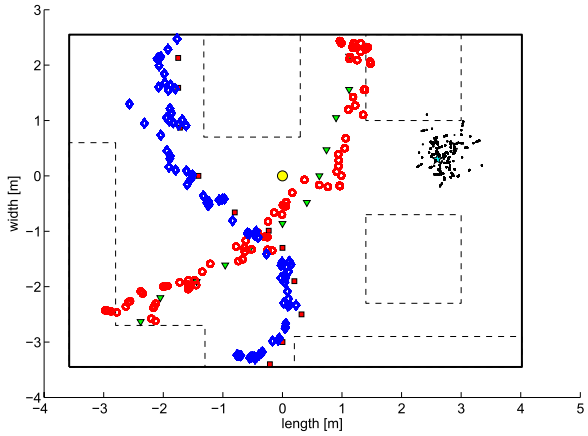

Fig. 11. Detection and tracking results in three occupants scenario.

The array consisted of eight elements of model SPM0204HD5 (see updated components in SPM family [35]) with an inter-element separation of 4.6 mm.

A. Granular Presence Sensing

The parameters of the transmitted waveform were $T_s = 4$ ms and $T_p = 60$ ms. Since the receiver uses two consecutive pulses for MTI processing, the time between scans is 120 ms. Parameter $\kappa_2 = 10$ was chosen which gives a latency of at least 1.2 s before the tracker initiates a target. Furthermore, $\kappa_1 = 30$ was chosen which indicates the tracker waits at least 3.6 seconds before a disappeared target is deleted. For real-time implementation, a granularity of 2 degrees was chosen for DoA estimation in both azimuth and elevation angles.

We consider the granular detection and tracking performance for two multiple occupant scenarios in an office as depicted in Figs. 8 and 10. The solid lines at the edges denote the physical boundaries, while the dashed lines indicate workspace regions and furniture. In the first scenario, one occupant moves along the track marked by the red squares while the second occupant follows the track marked by green triangles. Both occupants start simultaneously from the points A and B as depicted in Fig. 8, the occupant marked by the green triangles first passes the intersection as the occupant marked by the red squares follows. The results of the estimated trajectory upon detection and tracking are shown as black circles and blue diamonds for the first and second occupant respectively in Fig. 9. As can be seen, the estimated locations and track closely match locations along the real trajectory. The deviation from the true trajectory are caused close to the areas of dense local scattering (due to tables in the room).

In the second scenario, three occupants are present in the room as shown in Fig. 10. The first occupant indicated by the cyan star makes minor movements (e.g. small hand and body movements) while seated on a chair at the specified location. The two other occupants move along the tracks designated by the green triangles and red squares respectively. The second occupant starts at point A (following the green triangles trajectory); when the second occupant approaches the middle of its track, the third occupant starts from point B and walks along the red squares. The results from the real time location estimation are shown in Fig. 11 by black dots, red circles and blue diamonds for the first, second and third occupant respectively. The figure clearly shows that the real-time location estimates closely match the target trajectories.

There are a number of factors such as furniture in the space, ceiling mounting height of the sensor, radiation pattern of the transmitter and receiver elements of the ultrasonic

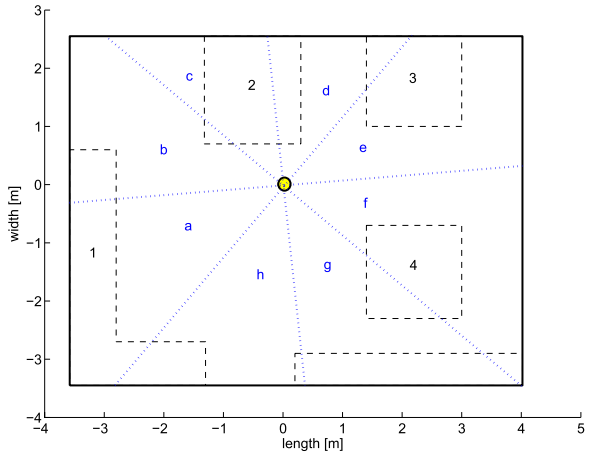

Fig. 12. Zoning of the test office room based on azimuth angle.

array, that affect the tracking performance within the sensing region. In the experimental setup, for the choice of the transmitter/receiver and ceiling height, detection performance deteriorates at the physical boundaries of the office space since the ultrasonic transmitter/receiver sensitivity is lower due to the beam angle characteristics.

B. Ultrasonic Control Messaging

The communication scheme was tested on three speakers of different laptop models, serving as the mobile device. The mobile device was placed at one of four possible workspaces (marked 1-4) as shown in Fig. 12, where the zones (marked a-h) are also depicted. The orientation of the mobile device was chosen such that a clear LOS path exists between the transmitter and the receiver array, for which a typical channel response resembles Fig. 5 (here reflections still exist for instance due to the screen of the laptop). A total of 150 message transmissions were done from the four workspaces and it was found that all messages were received correctly, and also identified in the correct zone. In order to also test the performance under adverse conditions, another scenario was considered by introducing non-LOS components (by pointing the transmitter away from the receiver, obscuring the LOS path). For this scenario, approximately 70% of the messages were received correctly. This degradation is due to intersymbol interference (ISI) and is expected. The performance can be improved by using transmission redundancy and advanced receiver processing (e.g. channel equalization). However, since only the LOS scenario was of interest in our application, we did not include such receiver processing in our design.

It was observed that the speaker hardware limitations, i.e. operating at a frequency of 20 kHz using commercial acoustic speakers, leads to a very minor buzz (a "tic" sound) when the speakers were at the highest volume. While unintentional, it has the advantage of providing feedback to occupants that a user is signalling so that simultaneous user control messaging may be avoided. There is still a small probability that due to multiple users signalling at the same time, some messages are lost. We expect that these situations occur in practice with very small probability and are resolved by social interaction among users and/or multiple signalling requests from users with random backoff times.

VI. Conclusion

An ultrasonic uniform circular array sensing and communication solution was proposed for granular occupancy detection and user messaging, with potential application in a smart lighting control system to achieve automatic as well as user-controllable localized illumination. The range, azimuth and elevation angles corresponding to potential occupant movements were obtained after range processing and DoA estimation. Kalman filter tracking based on an NCV model and track maintenance algorithms were employed to estimate movement tracks. User messaging was realized with acoustic device speakers operated at ultrasonic frequencies, and the same ultrasonic array presence sensor was reused as a communication receiver. A prototype of the proposed system with an 8-element circular array was implemented and shown to provide promising performance in an indoor office environment.

References

[1] Energy Information Administration. *Lighting in Commercial Buildings*. [Online]. Available: http://www.eia.gov/consumption/commercial/, accessed May 1, 2014.

[2] D. Caicedo and A. Pandharipande, "Distributed illumination control with local sensing and actuation in networked lighting systems," *IEEE Sensors J.*, vol. 13, no. 3, pp. 1092–1104, Mar. 2013.

[3] N. van de Meugheuvel, A. Pandharipande, D. Caicedo, and P. P. J. van den Hof, "Distributed lighting control with daylight and occupancy adaptation," *Energy Buildings*, vol. 75, pp. 321–329, Jun. 2014.

[4] Y.-J. Wen and A. M. Agogino, "Personalized dynamic design of networked lighting for energy-efficiency in open-plan offices," *Energy Buildings*, vol. 43, no. 8, pp. 1919–1924, 2011.

[5] A. Pandharipande and D. Caicedo, "Adaptive illumination rendering in LED lighting systems," *IEEE Trans. Syst., Man, Cybern., Syst.*, vol. 43, no. 5, pp. 1052–1062, Sep. 2013.

[6] M.-S. Pan, L.-W. Yeh, Y.-A. Chen, Y.-H. Lin, and Y.-C. Tseng, "A WSN-based intelligent light control system considering user activities and profiles," *IEEE Sensors J.*, vol. 8, no. 10, pp. 1710–1721, Oct. 2008.

[7] H. J. Keller, "Advanced passive infrared presence detectors as key elements in integrated security and building automation systems," in *Proc. IEEE Carnahan Conf. Secur. Technol.*, Oct. 1993, pp. 75–77.

[8] D. Caicedo and A. Pandharipande, "Ultrasonic arrays for localized presence sensing," *IEEE Sensors J.*, vol. 12, no. 5, pp. 849–858, May 2012.

[9] D. Caicedo and A. Pandharipande, "Ultrasonic array sensor for indoor presence detection," in *Proc. 20th Eur. Signal Process. Conf. (EUSIPCO)*, Aug. 2012, pp. 175–179.

[10] D. Caicedo and A. Pandharipande, "Distributed ultrasonic zoned presence sensing system," *IEEE Sensors J.*, vol. 14, no. 1, pp. 234–243, Jan. 2014.

[11] M. M. Saad, C. J. Bleakley, and S. Dobson, "Robust high-accuracy ultrasonic range measurement system," *IEEE Trans. Instrum. Meas.*, vol. 60, no. 10, pp. 3334–3341, Oct. 2011.

[12] M. M. Saad, C. J. Bleakley, T. Ballal, and S. Dobson, "High-accuracy reference-free ultrasonic location estimation," *IEEE Trans. Instrum. Meas.*, vol. 61, no. 6, pp. 1561–1570, Jun. 2012.

[13] C. Li, D. A. Hutchins, and R. J. Green, "Short-range ultrasonic digital communications in air," *IEEE Trans. Ultrason., Ferroelectr., Freq. Control*, vol. 55, no. 4, pp. 908–918, Apr. 2008.

[14] C. Li, D. A. Hutchins, and R. J. Green, "Response of an ultrasonic communication channel in air," *IET Commun.*, vol. 6, no. 3, pp. 335–343, 2012.

[15] W. Jiang and W. M. D. Wright, "Wireless communication using ultrasound in air with parallel OOK channels," in *Proc. 24th IET Irish Signals Syst. Conf.*, Jun. 2013, pp. 1–6.

[16] S. Holm, O. B. Hovind, S. Rostad, and R. Holm, "Indoors data communications using airborne ultrasound," in *Proc. IEEE Int. Conf. Acoust., Speech, Signal Process.*, Mar. 2005, pp. iii/957–iii/960.
[17] S. Holm, "Airborne ultrasound data communications: The core of an indoor positioning system," in *Proc. IEEE Int. Ultrason. Symp.*, Sep. 2005, pp. 1801–1804.
[18] H. Krim and M. Viberg, "Two decades of array signal processing research: The parametric approach," *IEEE Signal Process. Mag.*, vol. 13, no. 4, pp. 67–94, Jul. 1996.
[19] M. A. Richards, J. A. Scheer, and W. A. Holm, Eds., *Principles of Modern Radar: Basic Principles*. Hertfordshire, U.K.: SciTech Publishing, 2010.
[20] S. Blackman and R. Popoli, *Design and Analysis of Modern Tracking Systems*. Norwood, MA, USA: Artech House, 1999.
[21] S. Naghibzadeh, A. Pandharipande, D. Caicedo, and G. Leus, "Indoor granular presence sensing with an ultrasonic circular array sensor," in *Proc. IEEE Int. Symp. Intell. Control (ISIC)*, Oct. 2014, pp. 1644–1649.
[22] V. Filonenko, C. Cullen, and J. Carswell, "Investigating ultrasonic positioning on mobile phones," in *Proc. Int. Conf. Indoor Positioning Indoor Navigat.*, Sep. 2010, pp. 1–8.
[23] W. A. Arentz and U. Bandara, "Near ultrasonic directional data transfer for modern smartphones," in *Proc. Int. Conf. Ubiquitous Comput.*, 2011, pp. 481–482.
[24] P. Ioannides and C. A. Balanis, "Uniform circular arrays for smart antennas," *IEEE Antennas Propag. Mag.*, vol. 47, no. 4, pp. 192–206, Aug. 2005.
[25] C. A. Balanis, *Antenna Theory: Analysis and Design*, 3rd ed. New York, NY, USA: Wiley, 2005.
[26] M. A. Richards, *Fundamentals of Radar Signal Processing*. New York, NY, USA: McGraw-Hill, 2005.
[27] S. S. Blackman, "Multiple hypothesis tracking for multiple target tracking," *IEEE Aerosp. Electron. Syst. Mag.*, vol. 19, no. 1, pp. 5–18, Jan. 2003.
[28] Y. Bar-Shalom and X.-R. Li, *Estimation and Tracking: Principles, Techniques, and Software*. Boston, MA, USA: Artech House, 1993, ch. 6.
[29] R. Resnick and D. Halliday, *Fundamentals of Physics*. New York, NY, USA: Wiley, 1988.
[30] M. H. Hayes, *Statistical Digital Signal Processing and Modeling*. New York, NY, USA: Wiley, 2009.
[31] L. W. Couch, II, *Digital and Analog Communication Systems*. Englewood Cliffs, NJ, USA: Prentice-Hall, 2007.
[32] J. Heiskala and J. Terry, *OFDM Wireless LANs: A Theoretical and Practical Guide*. Indianapolis, IN, USA: Sams Publishing, 2001.
[33] T. Aguilera, J. A. Paredes, F. J. Alvarez, J. I. Suarez, and A. Hernandez, "Acoustic local positioning system using an iOS device," in *Proc. Int. Conf. Indoor Positioning Indoor Navigat.*, Oct. 2013, pp. 1–8.
[34] [Online]. Available: http://www.prowave.com.tw/english/products/ut/ep/40ep14d.htm, accessed May 1, 2014.
[35] [Online]. Available: http://www.knowles.com/eng/Products/Microphones/Surface-mount-MEMS, accessed May 1, 2014.

Shahrzad Naghibzadeh (S'14) received the B.Sc. degree in electrical engineering from the Ferdowsi University of Mashhad, Mashhad, Iran, in 2012, and the M.Sc. (*cum laude*) degree in electrical engineering, telecommunications, from the Delft University of Technology, Delft, The Netherlands, in 2014, where she is currently pursuing the Ph.D. degree. From 2013 to 2014, she was an Intern with Philips Research, Eindhoven, The Netherlands, working on localization and granular presence sensing with ultrasonic circular arrays for her master's thesis. Since 2012, she has been with the Circuits and Systems Group, Delft University of Technology.

Ashish Pandharipande received the B.E. degree in electronics and communications engineering from Osmania University, Hyderabad, India, in 1998, and the M.S. degrees in electrical and computer engineering and mathematics, and the Ph.D. degree in electrical and computer engineering from the University of Iowa, Iowa City, IA, USA, in 2000, 2001, and 2002, respectively. In 2003, he was a Post-Doctoral Researcher at the University of Florida. From 2004 to 2006, he was with the Samsung Advanced Institute of Technology as a Senior Researcher. He has held visiting positions at AT&T Laboratories, the Department of Electrical Communication Engineering, Indian Institute of Science, India, and Nanyang Technological University, Singapore. Since 2006, he has been a Senior Scientist with Philips Research, Eindhoven, Netherlands.

His research interests are at the intersection of sensing, networking and controls, and system applications in domains like intelligent lighting systems, energy monitoring and control, and cognitive spectrum sharing. He is currently an Associate Editor for the IEEE TRANSACTIONS ON SIGNAL PROCESSING and IEEE SENSORS JOURNAL, an Editor of the *EURASIP Journal on Wireless Communications and Networking*, and a member of the International Advisory Board, Lighting Research & Technology.

David Caicedo received the Engineer degree in electronics and telecommunications from ESPOL, Guayaquil, Ecuador, in 2006, the M.S. (*cum laude*) degree in electrical engineering, with a specialization in the field of telecommunications from the Delft University of Technology, Delft, The Netherlands, in 2010, and the Ph.D. degree in electrical engineering from the Eindhoven University of Technology, Eindhoven, The Netherlands, in 2014. As part of his engineering program he completed an internship at Nokia, Guayaquil, Ecuador, in 2006. From 2007 to 2008, he was with Nokia Siemens Networks as a Radio Frequency Engineer, Bogota, Colombia. He has been with Philips Research, Eindhoven, since 2009, working on his master's thesis from 2009 to 2010, on a van der Pol Ph.D. position until 2014, and since 2014, as a Research Scientist. His research interests are in the areas of sensor signal processing algorithms and applications, mobile wireless communications, and wireless networking.

Geert Leus received the M.Sc. and Ph.D. degrees in applied sciences from the Katholieke Universiteit Leuven, Belgium, in 1996 and 2000, respectively. He is currently an Antoni van Leeuwenhoek Full Professor with the Faculty of Electrical Engineering, Mathematics and Computer Science, Delft University of Technology, The Netherlands. His research interests are in the area of signal processing for communications. He is the recipient of the 2002 IEEE Signal Processing Society Young Author Best Paper Award and the 2005 IEEE Signal Processing Society Best Paper Award. He was the Chair of the IEEE Signal Processing for Communications and Networking Technical Committee, and an Associate Editor of the IEEE TRANSACTIONS ON SIGNAL PROCESSING, the IEEE TRANSACTIONS ON WIRELESS COMMUNICATIONS, the IEEE SIGNAL PROCESSING LETTERS, and the *EURASIP Journal on Advances in Signal Processing*. He is also a Member-at-Large of the Board of Governors of the IEEE Signal Processing Society and a member of the IEEE Sensor Array and Multichannel Technical Committee. He finally serves as the Editor in Chief of the *EURASIP Journal on Advances in Signal Processing*.